Performance Analysis of Onshore NB-IoT for Container Tracking During Near-the-Shore Vessel Navigation

Srikanth Kavuri, Dmitri Moltchanov, Aleksandr Ometov, *Member, IEEE,*
Sergey Andreev, *Senior Member, IEEE,* and Yevgeni Koucheryavy, *Senior Member, IEEE*

***Abstract*—This work aims to put forward the utilization of onshore Narrowband IoT (NB-IoT) infrastructure for tracking of containers transported by marine cargo vessels while operating near the coastline. We introduce and evaluate three connectivity strategies, including direct sensor-to-onshore base station (BS) transmission as well as two relay-aided schemes using dedicated vessel-BS or unmanned aerial vehicle (UAV)-mounted BS as intermediate nodes. To assess and compare the proposed schemes in terms of the message loss and delay metrics as well as sensor lifetimes, we first employ stochastic geometry to characterize the connectivity process with the onshore deployment and then resort to system-level simulations. Our results indicate that the direct access option suffers from the poorest performance. The relay-based alternatives allow to dramatically improve the system operation by effectively distributing the transmission requests over time at the relay side and thus mitigating contention. Further gains enabled with UAV relaying are due to extended coverage that increases the available BS density. The considered relaying operation may help tolerate intermittent connectivity across a broad range of system parameters.**

***Index Terms*—NB-IoT, cargo monitoring, marine vessels, UAV relaying, real-time tracking, performance assessment.**

I. Introduction

Contemporary trade flows significantly depend on the movement of physical containers all around the world. Container logistics [1] is currently accounting for approximately 90% of the global trade. As a result, any small lapse in this well-planned and carefully balanced mechanism can drastically affect the cost and customer satisfaction levels [2].

Up to 130 million fully-loaded containers are continuously handled by the maritime industry [3] as they are carried by more than 52,000 cargo vessels [4]. The market share taken by this transportation type has already approached US $17 trillion in 2017 and is only expected to grow further [5]. Evidently, some of the goods are being damaged or lost during transportation due to adverse weather conditions among other reasons. According to [6], the corresponding losses exceeded 20% in 2017. The proportion of delivered containers experiencing minor damage is also high [7]. Therefore, their monitoring and tracking is a crucial task for the modern maritime industry. Consequently, technology investments have been increasing from 2014 to 2016, with the Internet of Things (IoT) sensor and monitoring solutions facing the most significant growth at 19%, followed by data loggers at 14%, as well as Global Positioning System (GPS) and satellite radio at 5%, according to a survey in [8]. Many industrial methods aim at in-sea tracking, but most of those are based on the relatively expensive satellite technology [9].

Meanwhile, the IoT communications sector has evolved dramatically over the past decades [10]. This transformation has converted the IoT technology from simple, limited, and single-purpose proprietary solutions, such as SigFox [11] or ZigBee [12], to globally-standardized and uniform systems, such as Narrowband IoT (NB-IoT) technology proposed by 3GPP for future cellular networks [13], [14]. The NB-IoT is implemented in the licensed LTE bands [15] and may operate in standalone, guard-band, and LTE in-band modes. In NB-IoT, the primary resource block of 180 kHz is channelized into 12 subcarriers by 15 kHz each. It employs QPSK modulation, OFDMA access in the downlink, and SC-FDMA scheme in the uplink. Unlike legacy LTE, NB-IoT has three coverage enhancement levels (CE0 – 144 dB, CE1 – 154 dB, and CE2 – 164 dB); the uplink and downlink data is repeated 128 and 2048 times, respectively, in case of poor coverage. NB-IoT offers 15 km of coverage with 164 dB maximum coupling loss (MCL), which is 20 dB better compared to the legacy Global System for Mobile Communications (GSM). The resultant data rates are up to 250 kbps for multi-tone and 20 kbps for single-tone transmissions. Due to cellular layout in licensed bands, interference is significantly lower as compared to other systems, while data encryption and authentication mechanisms are in-built. Theoretically, NB-IoT may support up to 55K devices per cell, and its maximum latency is up to 10 seconds [16]. Based on its exceptional coverage and communications flexibility [17], [18], NB-IoT can be considered as an attractive candidate technology for container vessel monitoring.

Since cargo ships operate in close-to-the-shore areas for a significant time, see Fig. 1, we envision that the NB-IoT technology may be utilized for tracking their carried containers. In this work, we introduce and analyze three connectivity strategies, which include a direct access scheme where sensors communicate with the onshore network infrastructure directly, and two relaying schemes where either ship-mounted or UAV-deployed base stations (BSs) serve as a relay [19], [20]. The main findings of our study are:

- message loss performance of the direct access scheme is unacceptable for the practical ranges of system parameters; the major reason is in enforced synchronization between the sensors accessing the NB-IoT channel induced by long outage periods;
- the use of relaying schemes allows to considerably improve the system performance by effectively distributing the transmission requests over time at the relay air inter-

Correspondence email: dmitri.moltchanov@tuni.fi
Manuscript received June 12, 2019; revised December 19, 2019.

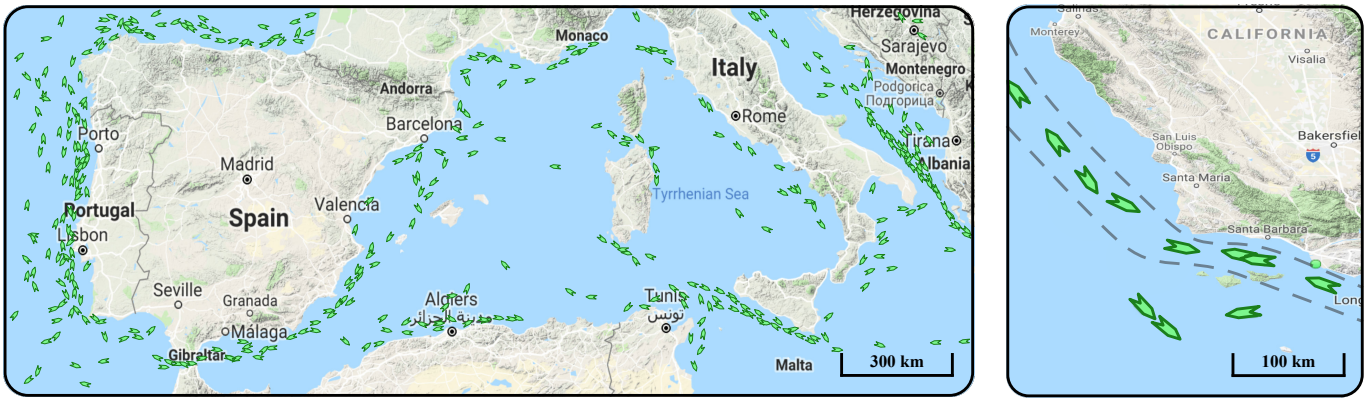

(a) Mediterranean sea cargo vessel routes

(b) Cargo vessel routes near California

Fig. 1. Example cargo vessel routes. Source: https://www.marinetraffic.com/, Date: Feb, 2020.

face and then further benefiting from mitigated contention at the onshore BS air interface;

- the utilization of UAV relaying further enhances the performance of this system by greatly increasing the number of onshore BSs available for concurrent connectivity.

The rest of this text is organized as follows. First, we provide a brief overview of the state-of-the-art technology employed in marine container tracking systems in the following section. We overview the state-of-the-art and related challenges as well as introduce our system model and outline the proposed connectivity schemes in Section II. Further, we provide an overview of the NB-IoT random access energy-saving capabilities in Sections III and IV. In Section V, we analyze the considered connectivity schemes for the performance metrics of interest. Our numerical assessment is conducted in Section VI. Conclusions are drawn in the last section.

II. Related Work and Challenges

A. Container Tracking and Monitoring Systems

Monitoring systems are constantly developing as part of e-Navigation, which is currently being developed by UN-chartered International Maritime Organization (IMO) and International Association of Lighthouse Authorities (IALA) starting as early as in 2005. Historically, IMO decided to include a well-defined strategy to integrate new and existing navigational tools for enhancing handling and safety of ships at the sea. Since then, many industrial giants are currently providing monitoring and tracking services for containers at sea. For example, Maersk is primarily focused on satellite communication to relay the data from its smart containers [21]. Here, GPS enables global tracking, while a modem and a SIM card facilitate the collection, storage, and sharing of the atmospheric conditions and power status. A satellite transmitter mounted on 400 of Maersk Lines vessels picks up the data streaming from the modem and sends it in real-time to a satellite that beams it back to the Remote Container Management (RCM) centers located around the globe.

Similarly to Maersk, Vobal Technologies rely upon a combined use of a GPS/GSM transmitter to deliver the data to the cloud. This solution employs the vessel as a wireless relay for transmitting the data from containers equipped with short-range wireless communication modules [22]. The operation is based on creating a local wireless network on-board the ship, thus enabling containers fitted with GPS/GSM modem devices to continue reporting while the vessel is on the water. ORBCOMM [23] provides another solution based on a coupling of GPS and GSM. This company offers a container tracking and monitoring system allowing to acquire full container visibility with real-time GPS location, motion detection, geofence management, and off-power operation. The solution is achieved by utilizing relaying via a ship-mounted BS. A similar service named ZIMonitor (utilizes RFID and GPS) is being offered by the company ZIM Integrated Shipping Services Ltd. [24]. The network infrastructure for this solution facilitates not only monitoring but also two-way control capabilities. We emphasize that may vendors and suppliers consider semi-centralized solutions based on deploying a BS on the ship.

Container tracking and monitoring systems recently attracted significant interest of the research community. The authors in [25] addressed and analyzed real-time monitoring solutions based on IEEE 802.15.4 technology for providing connectivity inside and between the containers as well as GSM/UMTS technology for constructing data links with the cloud. In [26], IEEE 802.11 radios were exploited for local on-board monitoring, while GPRS was used for connections with the mainland. Research in [27] proposed to use the widely adopted automatic identification system (AIS) for container tracking as a supplement for satellite-based options.

Based on this brief overview, one may classify the considered systems into two broad groups: (i) direct satellite/GSM tracking and (ii) shorter range tracking with aggregation and relaying. The advantages of conventional techniques, where each container is equipped with a long-range wireless module, e.g., GPS and/or GSM [28], include deep market penetration and off-the-shelf availability. Also, these do not require additional infrastructure, offer high positioning accuracy, and feature widely adopted software for visualization and management.

These systems are often offered on a per-subscription basis with the prices ranging from $7 to $30 per month, including portal and software access. From the technical perspective, they demand a line-of-sight (LoS) connection to the satellite,

which is somewhat challenging to achieve as containers are often stored on top of each other. On the one hand, the link is required to collect the location data, while on the other hand, one needs to keep the communications with the satellite (for satellite-based tracking solutions). Finally, the energy efficiency of sensors may be compromised since the utilization of satellite links is extremely power-hungry. The use of relaying strategies brings additional advantages to the considered system. The main expected benefits are related to the pricing policy that may allow for decreased subscription fees, lower hardware costs owing to globally-unified technology, longer sensor lifetimes due to smaller transmit power, etc. So far, the research community has not been deeply engaged in developing effective solutions for future container tracking and monitoring systems. In this work, we aim to shed light on the potential benefits of the emerging cellular NB-IoT infrastructure for such applications.

B. State-of-the-Art of UAVs for Maritime Industry

Indeed, the operation of UAVs in territorial waters may seem unacceptable in many countries without a license. In addition, complicated and harsh conditions, such as windy or rainy weather, may also become a major limitation for one of the considered system architectures. We believe that there are two perspectives on this problem. On the one hand, the regulations for the use of drones are, in fact, currently under preparation in most countries. For example, detailed regulations are still not present for UAV flights in the cities despite the fact that several large companies such as Amazon and Google are investing significant funds into various security and delivery related projects.

On the other hand, near-the-shore waters usually receive special treatment, and this may also be the case for the use of ship-mounted drones for navigation and communications purposes. In fact, the number of unmanned aerial systems (UASs) or UAV systems applications grows tremendously [29]. The increasing use of drones is supported by regulators, such as the European Maritime Safety Agency (EMSA). As an example, EMSA's Remotely Piloted Aircraft Systems Services (RPAS) are currently in use by the Croatian authorities to assist them with a range of coast guard functions, including vessel traffic monitoring, search and rescue, as well as the detection and monitoring of marine pollution. A request made in February 2019 by the Ministry of the Sea, Transport and Infrastructure of Croatia is aimed for the addition of vertical take-off and landing to existing observation mechanisms [30].

UAVs are also used for the inspection of ships to facilitate the ship repair and maintenance. Project RECOMMS (Remote Evaluation of Coatings and Corrosion on Offshore Marine Structures and Ships) is aiming to assist the offshore structures and ship inspection where manual checks are dangerous or even impossible. The RECOMMS team envisions that manual human inspections will be replaced by routine remote drone inspections providing real-time data to office-based staff and superintendents [31]. Project High EYE is also used for inspection of offshore wind turbines. The designed UAV allows to operate in inclement weather [32].

Already in 2017, Martek Aviation aimed to provide end-to-end service solutions for offshore applications such as search and rescue; detection and monitoring of illegal pollution; detection of drug and human trafficking; fisheries protection; and inspection of marine assets and infrastructure [33]. NorShipping project by Wilhelmsen Ships Service (WSS) develops a UAV-based system allowing for rapid delivery of parcels to ships [34]. A new market niche of drone delivery thus enables to decrease the urgent delivery price from US $1500 to only $150.

Another Canada-based project called RAVEN (Remote Aerial Vehicle for Environment-monitoring) focuses on new, cost-effective technologies for commercial maritime Intelligence Surveillance Reconnaissance (ISR) missions [35]. Further, project Loon Copter [36] is a hybrid unmanned aquatic–aerial quadcopter with active buoyancy control. It uses a ballast system to control buoyancy and depth underwater, as well as to achieve smooth transition of air-water and water-air. The closed-loop control algorithm is used to ensure stability and maneuvering of the vehicle's air and water surface, and the open-loop control algorithm is used for underwater maneuvering. Another active project, "Autonomous and Collaborative Offshore Robotics (aCOLOR)" [37] employs UAVs along with Unmanned Surface Vessel (USV) and Autonomous Underwater Vehicle (AUV) to achieve fully autonomous maritime operation in the air, underwater, and on the surface. The goal of the project is to create an autonomous robotic system to enable full-scale operation from obstacle detection to path planning. The ISM band is utilized for communications along with directive antennas allowing for high throughput communications in unlicensed bands.

It is important to note that windy and stormy weather is challenging for UAV operation. Today, many companies develop their systems to enable efficient UAV functioning in maritime conditions. For example, SAAB initiated work on Skeldar V-200 project in 2004 with the first prototype released in 2006 [38]. The major UAV tasks include surveillance, reconnaissance, target attainment, and transfer of target data to strike platforms. The UAV is also used for instant battle damage assessment and control of indirect fire.

The UAV-aided system can be used for logistics support and ship-to-ship or ship-to-shore operation in rough weather conditions. The data packets are relayed via a dual command and control data link operating in L, C, or S-band, as well as a sensor data link. The US Navy planned to utilize Triton UAV for maritime surveillance since 2017 [39] and, in September 2019, two high-altitude MQ-4C Triton drones were sent to Guam for their first overseas deployment [40]. On top of the proprietary communication system, the UAVs are equipped with AIS and multifunction active sensor radar for target detection and tracking.

As the number of such examples increases worldwide, there is solid ground to believe that the use of UAVs may become popular thus affecting the state decision with respect to allowing drones flights in specific locations. Based on the above survey, we conclude that maritime utilization of UAVs is a promising area since many active industrial and academic projects already develop various solutions to enable

UAV operation in complex weather conditions and with a heavy payload. Addition of a wireless relay module to the said system might be a promising step for system architects that aim at covering broader market of UAV applications.

C. Features of UAV Maritime Operation

Operation in windy and harsh conditions is one of the main features of maritime UAV systems affecting not only the flight but also the take-off and landing of the UAVs. Many researchers have studied the strategies and phases related to the flight cycle of the maritime UAV flight span. In this section, we overview some of the strategies and lessons learned from these studies.

The first group of challenges is related to the most complicated phases of launch and take-off from both moving and static platforms/vessels. Indeed, since most of the vessels do not have a long runway, engineers invested much effort into developing solutions explicitly accounting for the motion of the ship caused by both mobility and waves. Launch strategies of today are mainly settled and depend on the UAV type, including the rotary wing, e.g., vertical take-off (VTOL) [41], fixed-wing, e.g., rocket booster [42], bungee cord/catapult [43], hydraulic/pneumatic launchers [44], and other specific cases, such as parasail [45], balloon [46], etc.

UAV landing is another important aspect of the system operation. In practice, pilots spend countless hours practicing touchdowns because of the risk involved during the landing phase. Developing autonomous landing techniques has been an active direction of research over the past decade. In particular, UAV recovery solutions over water usually comprise of ship-based elements and UAV-based ones. The ship-based elements may include either a landing platform or a robot arm that holds a capture mechanism over the side of the ship, which compensates for wave-induced ship motion. There are works focusing on mechanical capture, such as net recovery [47], [48], arresting line [49], sky hook [50], as well as various active stabilization-based options also including platform-based [51], [52], [37]. Out of the above, VTOL has the least impact on the vessel's surface type.

Once the take-off and landing phases are understood, another significant phase related to maritime operation comes in focus – in-flight stabilization due to harsh weather conditions and real-time path finding. Evidently, most of the modern UAVs are equipped with several sensors aiming at improving the reliability and fault tolerance of such expensive equipment. Notably, the operation of fixed-wing UAVs is well studied and settled topic due to its roots coming from the military domain [53]. The operation of rotor-based small UAVs is however more affected by the wind [54], [55]. Wind dynamics may also impact the trajectory path of the UAV. The strategies for improving stabilization in these conditions are addressed by several studies, see, e.g., [56], [57].

Another issue of the operation over the sea is potential connectivity losses due to high waves. The study in [58] provides an overview of an intelligent strategy suitable for the UAV recovery in the case of connectivity loss. Many other investigations focus on specific challenges related to the UAV operation including midair collisions [59], impact of atmospheric icing [60], imagery retrieval [61], etc. Those, however, go beyond the scope of this paper. Generally, most of the UAVs used for maritime operation should overcome the above-listed challenges by design, thus providing a vast frontier to be utilized as relays in future monitoring systems.

D. NB-IoT Performance

There is a number of studies on NB-IoT performance evaluation focusing on both analysis and measurement campaigns. The pioneering work in [62] assesses the performance of the NDSCH channel. Particularly, it shows that the peak throughputs in both downlink and uplink are lower than the standardized 250 Kbit/s when the time offsets between DCI, NPDSCH/NPUSCH, and HARQ acknowledgment are considered. From the coverage perspective, the work reports 170 dB coupling loss compared to Rel-12 142 dB coupling loss. It also concludes that ten years of battery life can be theoretically reached if the UE transmits 200 bytes of data per day. The authors of [63] analyze the deployment specifics of the NB-IoT system. The work in [64] provides coverage and capacity analysis of NB-IoT and LTE-M technologies in a rural area. The authors of [65] focus on model design and realization, aiming at physical layer characteristics of NB-IoT. The correlated uplink and downlink characteristics are achieved for a model based on the LTE network. The simulation results have verified the NB-IoT performance expected by 3GPP that NB-IoT uplink time delay is lower than 10 s, channel utilization is higher than in LTE network, and coverage area is significantly broader than in LTE network. The work in [66] presents uplink coverage performance analysis for two extreme channel conditions. The results were verified using real-life measurements of NB-IoT testbed implementation.

A direct comparison between mMTC technologies has been performed in several studies. Notably, the authors in [67] and [68] conducted massive trials of the coverage assessment GPRS, NB-IoT, LoRaWAN, and SigFox technologies in almost $8,000$ km^2 rural area by showing that in most conditions NB-IoT outperforms its counterparts in terms of coverage. The study in [14] contributes a comparison of LoRaWAN and NB-IoT technologies from both technological and cost perspectives. It claims the NB-IoT maximum range of 35 km.

The study in [69] discusses the coverage extension of LPWAN systems using a Low Earth Orbit (LEO) satellite constellation. The transmission complies with the UE specifications standardized as NB-IoT by 3GPP in Release 13. This radio technology is an update of the LTE standard with enhanced performance: the supported path loss can be 20 dB higher than that with legacy LTE. A comparison between eMTC and NB-IoT operating in the LTE band for smart city applications is further performed in [70]. The authors evaluate the power consumption of both technologies and demonstrate that the battery lifetime of eight years could be achieved in a poor coverage scenario with the reporting interval of one day.

From the industrial perspective, Nokia Bell Labs have also provided their analysis of the NB-IoT system in [71] by outlining its design and discussing the important issues related

to the in-band deployment of NB-IoT in an LTE network. Deployment of NB-IoT in a limited number of cells instead of full coverage can cause coverage problems due to both high path loss and interference. Simulation results demonstrate that the increased co-channel interference with such a partial deployment in synchronous networks can be mitigated through PRB blanking in non-NB-IoT cells. Another study by Nokia in [72] confirms the achievability of NB-IoT requirements including low-cost devices, high coverage (20 dB improvement over GPRS), long device battery life (more than 10 years), and massive connectivity.

III. System Model

In this section, we specify our system model by introducing its essential components. We start by describing the deployment of interest and proceed with the target communication scenarios. Finally, we identify our metrics of interest.

We consider typical container ship routes along the shore, as demonstrated in Fig. 2. In addition to general sea lane cases, this scenario also suits for cabotage vessel operation, i.e., for shipment of cargo between a nation's ports, also called coastwise trade. The coastline is expected to be irregular, while the average distance to the coast is assumed to be constant and equal to d kilometers. We focus on a tagged cargo vessel moving along the route at the speed of v km/s. It is expected to carry N containers, each equipped with a sensor having the NB-IoT radio interface. We assume that the onshore NB-IoT BS locations organize a spatial Poisson point process (PPP) with the density of λ_B BSs per square kilometer. The NB-IoT BSs operate in a standalone regime over 900 MHz band [15]. The standard path loss for 900 MHz band is further employed to determine the coverage distances in Fig. 2 [15] as $L = l + 37.6 \log_{10} x$, where x stands for the cell radius in kilometers, while the reference coefficient l is 120.9 for the 900 MHz band.

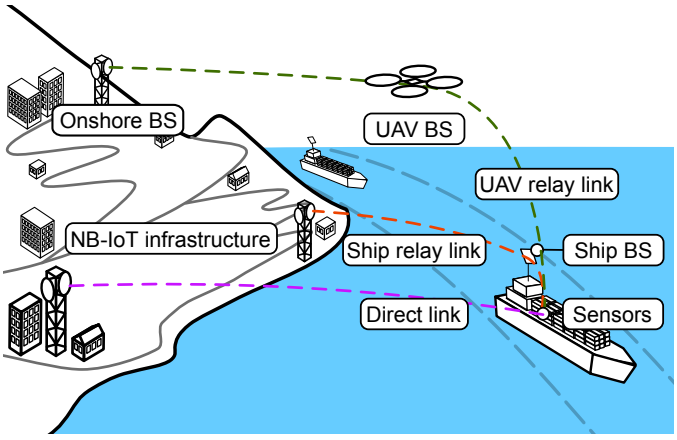

Fig. 2. Considered cargo vessel deployment and communication scenarios.

The vessel is also equipped with an NB-IoT BS that may act as a relay for the messages from on-board sensors to the onshore NB-IoT infrastructure. Another option is that a cargo vessel may operate a small fleet of drones (or utilize those in use for coastal guard services), also equipped with NB-IoT interfaces. These UAVs may serve as additional relays to provide coverage extension. In the considered deployment, we assess the following three alternative communication schemes:

- *Direct Access (DA).* In this baseline scheme, the on-board sensors attempt to transmit directly to the onshore BS. This scenario is mainly limited by the transmit power of a sensor that could be directly interpreted as energy consumption or sensor lifetime.
- *Ship Relaying (SR).* In this scheme, the vessel is assumed to be equipped with a BS unit capable of retransmitting the sensor messages to the onshore BS. This option not only promises better energy consumption as compared to DA but also enables favorable conditions during the randomized channel access procedure.
- *UAV Relaying (UR).* In the third scheme, a cargo vessel operates the UAVs equipped with the NB-IoT BSs that serve as relay nodes. UAVs flying close to the coastal line offer additional coverage, thus effectively increasing the number of onshore BSs available for establishing connections. This scheme may also be of interest if the vessel is farther away from the shore, which can cause complete or partial connectivity loss and result in significant sensor battery drains.

Each sensor is assumed to generate a message each T seconds. To ensure that there are no outdated messages in the system, the lifetime of a message equals the inter-message arrival time, T. That is, if a message is not delivered successfully during T, it is considered to be discarded (or lost permanently). As the numbers of containers on modern cargo vessels are rather large and may reach a few thousand items [73], we employ the superposition property of point processes and represent the message arrival process from sensors by using a Poisson process with rate λ [74].

We consider the standardized NB-IoT operation on every radio interface of the system. Accordingly, the overall procedure can be divided into two phases (i) random access phase and (ii) transmission phase. Upon new message generation, the sensor attempts to detect the broadcast signal from the NB-IoT BS, during which the access barring status, the cell identifier (ID), and the tracking area code will be decoded. The primary and secondary synchronization signals are used for channel acquisition. If there is a BS in coverage, it provides scheduling information (time and frequency resources) to all its devices. The sensor decodes the Master Information Block (MIB) and the Signaling Information Block (SIB), as well as advances the time to conduct its transmission over the designated channel.

The BS decodes uplink messages and resolves any initial contention if multiple devices transmit over the same time and frequency. If no collision, the BS returns the uplink scheduling information to the sender. The sensor then transmits on the upper link scheduling information to establish a session. If two sensors communicate over the same resources, the BS decodes only the original sender and discards the duplicate user access. Upon acquiring its uplink resources, the sensor makes a transmission based on the Narrowband Physical Downlink Control Channel (NPDCCH) repetitions designated for the coverage enhancement (CE) level. The NB-IoT random

access procedure is described in more detail in Section IV. Once access is granted, a data transmission phase is initiated.

Since onshore NB-IoT infrastructure is not always available in the described system, the random access procedure is expected to become a bottleneck for the considered connectivity schemes [75]. Therefore, the primary metrics of interest are the message loss probability and the mean delay experienced by the messages. Note that losses may occur in our considered system as a result of either reaching the maximum number of retransmission attempts or message lifetime expiration. The mean delay is conditioned on the successful message delivery.

In this paper, we concentrate on the access phase as the one having the most impact on the system performance. Parameterizing the NB-IoT operational regime such that the highest possible communications range is provided for different identified strategies, the crucial parameters affecting the performance of the proposed strategies are as follows: (i) the message arrival intensity measured in message/hours/container, (ii) NB-IoT BS intensity in units/km^2, and (iii) the number of preamble retransmissions, M [76]. Once access is granted, the message is transmitted without contention. Therefore, we study how a wide range of these input parameters affects the message loss probability, mean delay, and mean sensor lifetime as the main metrics identified to be the key performance indicators (KPIs) in ISO/TS 18625 [77].

IV. NB-IoT Capabilities and Features

In this section, we first provide a technical background on the NB-IoT random access procedure and energy-saving capabilities. A simplified overview of these features is available in, e.g., [78], [72]. Then, we use an appropriate propagation model to parametrize the considered connectivity schemes.

A. Random Access Procedure

Access to the shared medium in NB-IoT is based on a random access procedure facilitated by a new single-tone signal with frequency hopping of the NB-IoT Physical Random Access Channel (NPRACH). Transmitting a random access preamble is the first step of the random access procedure that enables a User Equipment (UE) to establish a connection with the network. Acquiring uplink timing is another main objective of random access in Orthogonal Frequency-Division Multiple Access (OFDMA) systems. The acquired uplink timing is used to command the UE to perform timing advance to achieve uplink synchronization in OFDMA systems. Particularly, a preamble is transmitted whenever the UE requests access to the channel. It consists of symbol groups transmitted on a single subcarrier containing a Cyclic Prefix (CP) followed by five symbols. The contents of a preamble is generated from Zadoff-Chu sequences with a zero correlation zone produced by one or several root sequences [79]. Two preamble formats, which differ in the CP length, are defined for NB-IoT. A random-access preamble comprises 67 μs CP for *format 0* and 267 μs for *format 1* followed by five symbols having the duration of 1.333 ms, which gives the total length of 1.4 ms and 1.6 ms, respectively.

The preamble is divided into four groups of symbols transmitted without gaps during an attempt. Further, frequency hopping is applied to each group of symbols to ensure that they are transmitted on different subcarriers. When 15 kHz subcarrier spacing is used, such hopping is restricted to the set of 12 neighboring subcarriers. In case of 3.75 kHz subcarrier spacing, NPRACH resources can occupy 12, 24, 36, or 48 subcarriers. A random access preamble may be repeated 1, 2, 4, 8, 16, 32, 64, or 128 times depending on the coverage level and using the same power for each transmission. Also, the periodicity of preamble transmissions varies according to the selected CE level with the values from 40 ms and up to 2.56 s. The starting time of a channel access preamble within a period is defined by the evolved Node B (eNB).

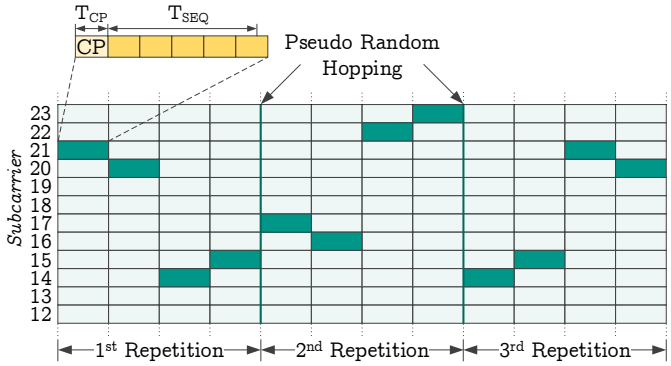

Fig. 3. NPRACH preamble repetition procedure.

The UE is allowed to select among 12 possible subcarriers for its preamble transmission, as illustrated in Fig. 3. In the ordered transmission case, the first symbol group of the preamble is conveyed on a subcarrier defined by the eNB. Otherwise, the UE selects a subcarrier for the first symbol group randomly. The remaining three symbol group subcarriers are determined by an algorithm that takes into account only the location of the first symbol group. For the selection of a subcarrier of the first symbol group in the subsequent repetitions, pseudo-random hopping is applied where N_{ID}^{NCell} and the repetition number are used as input data. The choice of subsequent subcarriers for the remaining symbol groups is again dependent only on the first symbol groups. The utilized frequency hopping algorithm is designed in a way that any selection of the first subcarrier leads to hopping schemes that never overlap.

The RACH procedure in NB-IoT always starts with the transmission of a preamble, as mentioned above. When the Random Access Response (RAR) is received from the eNB, a scheduled message is transmitted to begin a connection resolution procedure. Finally, the Connection Resolution (CR) message is sent to the UE during the last step as an indication of the RACH process completion. After a preamble transmission, the UE calculates its Random Access and Radio Network Temporary Identifier (RA-RNTI) from the transmission time. Then, the UE checks the PDCCH for Downlink Control Information (DCI) format N1 scrambled with RA-RNTI for the RAR message. This message should arrive within the Response Window (RW), which starts within 3 subframes (SFs) after the last preamble.

TABLE I
RU OPTIONS FOR NPUSCH FORMAT 1 WITH 15 KHZ SPACING.

Subcarriers	Slots	Duration
1	16	8 ms
3	8	4 ms
6	4	2 ms
12	2	1 ms

TABLE II
*e*DRX CYCLE LENGTH COMPARISON.

Cat M1 (seconds)	NB-IoT (seconds)
5.12	20.48
10.24	40.96
20.48	81.92
40.96	163.84
81.92	327.68
163.84	655.36
327.68	1310.72
655.36	2621.44
1031.72	5248.88
2621.44	10485.76

If the associated RAR was not received, then the UE transmits another Random Access Preamble (RAP) message. Preamble transmission can be attempted up to the maximum number of repetitions as defined in the CE level of the UE. When the maximum number of repetitions is reached without success, the UE proceeds to the next CE level if such next level is available. Otherwise, an eventual failure is reported to the Radio Resource Control (RRC). If the RAR is received, the UE obtains the timing advance command that allows the following message to be time-aligned. Such time alignment is also required for the transmission over the Narrowband Physical Uplink Shared Channel (NPUSCH). Finally, the RAR grants access by providing with all the relevant information for data transmission.

For the uplink data transmission, only NPUSCH is utilized, which also includes Uplink Control Information (UCI) using a different format. The transmission relies upon Single Carrier Frequency Division Multiple Access (SC-FDMA) either with 3.75 kHz or 15 kHz subcarrier spacing. The difference in the subcarrier spacing also impacts the resource grid for transmission. For the 15 kHz spacing, one Time Slot (TS) is 0.5 ms long in contrast to 2 ms in case of 3.75 kHz subcarrier spacing. However, the overall structure of a slot remains the same for both spacings and consists of 7 OFDM symbols.

Two formats are defined in NPUSCH. The first one is used for data transfer with the transport block limited to 1000 bits, while the second one carries UCI, which is restricted to acknowledgments of the downlink transmission. The smallest unit to map a transport block is a Resource Unit (RU) with a variable size that depends on the NPUSCH format and the subcarrier spacing. NPUSCH *format 1* with 3.75 kHz spacing defines the RU with one subcarrier and 16 slots in the time range with the total length of 32 ms. For 15 kHz spacing, four possible variations of RU are defined as listed in Table I. For NPUSCH *format 2*, only one RU is specified having the length of 4 slots, which implies 8 ms duration of the RU in case of 3.75 kHz spacing as well as 2 ms for 15 kHz subcarrier spacing. NPUSCH *format 2* also supports only one modulation scheme utilizing BPSK, while *format 1* modulation depends on the selected RU. For RUs with one subcarrier, BPSK and QPSK modulations may be employed.

Permission for all uplink data transfers is granted in NPDCCH via DCI format N0. The start time of NPUSCH, the number of repetitions, the number of RUs used in the transport block, the MCS, and the number of subcarriers together with their position over the frequency range are indicated as well. The time data for OFDM modulation is created by applying an Inverse Fast Fourier Transform (IFFT) and by placing a CP in front of the symbol. When 15 kHz subcarrier spacing is used, the CP is the same as in LTE, i.e., 4.7 μs, which corresponds to 144 samples. For 3.75 kHz spacing, the CP consists of 256 samples with a total length of 8.3 μs. In case of the latter, 2304 samples having the duration of 75 μs at the end of each slot remain empty, thus serving as a guard interval.

Another functionality related to the uplink channel is Demodulation Reference Signal (DMRS), which is multiplexed together with the data; therefore, it is sent only in the RUs containing data transmission. The purpose of DMRS is to estimate the channel conditions and to ensure coherent demodulation. Depending on the selected NPUSCH format, DMRS is reported in one (NPUSCH *Format 1*) or three (NPUSCH *Format 2*) SC-FDMA symbols, while its position in the resource elements also depends on the subcarrier spacing. The contents of the DMRS symbols are constructed from a base sequence and then multiplied by the phase factor.

B. Energy Consumption

The 3GPP has specified two power conservation options for the NB-IoT, power-saving mode (PSM) and extended discontinuous reception (eDRX) mode. The PSM mode, see Fig. 4, is described in 3GPP TS 23.682 (Rel. 12). It is applicable for a static device that does not require continuous connectivity. Since PSM has no support in the circuit-switching domain on the network side, it should only be used by the UEs operating in the message switching domain. As illustrated in Fig. 4, there are three stages in the PSM. In Active cycle, the UE transmits its data and then changes the status to receive (idle) during

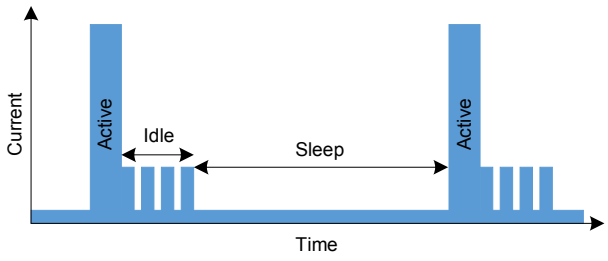

Fig. 4. Power saving mode operation.

which it decodes the incoming messages. If no further action is required, the device enters a sleep mode.

The BS supporting the PSM will acknowledge its usage and provide the active time value to the end device. The paging window remains constant, but this parameter can be extended by the network provider accordingly. The LTE core network registers the active time value assigned to the end device; it can be updated when the UE is willing to modify it. While the device is in a sleep period, the BS will accumulate the incoming messages and push them to the end device once it is activated. The UE can sleep for a maximum of 413 days, and the maximum awake time is 186 minutes.

The eDRX mode, see Fig. 5, is an advancement in power conservation methods where the end device periodically enters an idle mode to listen to the incoming messages instead of directly initiating the active cycle. Hence, there is a lag in listening to paging messages. This mode suits better for the cases where the UE moves and needs to establish connections frequently. The BS will still buffer the incoming data until the end device is connected. Table II shows the eDRX cycle length comparison between LTE M1 and NB-IoT. Due to longer eDRX cycles, NB-IoT devices have better lifetimes compared to LTE M1 devices.

C. Power Budget and Coverage

Following 3GPP, the transmit power at the NB-IoT BS is 43 dBm. We assume zero antenna gains as well as apply the general link power budget equation in the following form

$$L_P = 174 + P_T + G_T - L_T - S_{\min} - L_P - \\ - N_F + G_R - L_R, \quad (1)$$

where the downlink maximum coupling loss (MCL) is 164.44 dB, which is 20 dB better compared to the GPS signal; it is the highest among those offered by the IoT technologies (see Table III for input parameters). In practice, signal penetration is sufficiently deep, such that it can reach indoors and go inside basements being the best candidate as compared to GPRS, LoRa, and SigFox [67].

Applying the free-space path loss model in the form

$$L_P = 32.44 + 20\log_{10} x + 20\log_{10} f_c, \quad (2)$$

where f_c is the carrier frequency in MHz and x is the distance in kilometers, one may estimate the downlink coverage of the BS. Fig. 6 illustrates the downlink coverage distance for

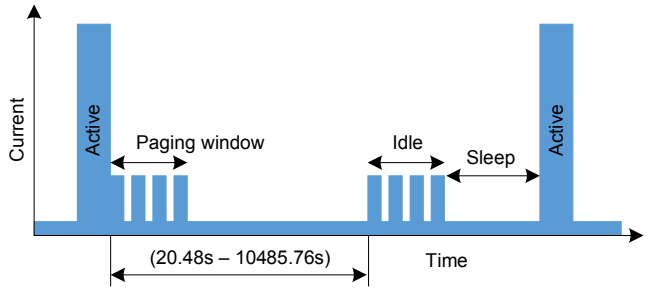

Fig. 5. Extended discontinuous reception mode.

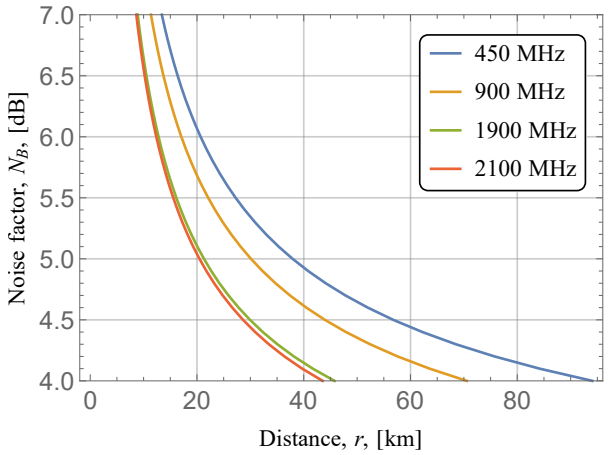

Fig. 6. Downlink coverage of NB-IoT.

different frequency bands. In urban areas where the noise factor, N_F, is high, the coverage is expected to remain rather limited, especially in 1900 MHz band where it is right below 10 km. In our study, the coastal area is assumed to have no irregular blockage and can be considered as a rural territory. At $N_F = 5.0$, the coverage is about 22 km with the transmit power budget of 43 dBm. The lower bands provide even better coverage, but the data rates are reduced accordingly. When there are no obstacles or the noise factor is less than 5.0, NB-IoT downlink may scale up to 40 km.

In the uplink, NB-IoT supports the following granularity: (i) single tone (either 3.75 kHz or 15 kHz) and (ii) multi-tone (3.75 kHz and 15 kHz). Following 3GPP, the transmit power of the NB-IoT device is limited to 23 dBm. Applying (1), the MCL is 164.25 dB and 158.23 dB for 15 kHz and 3.75 carrier bandwidths, respectively (see Table III for input parameters). Fig. 7 highlights the uplink coverage of NB-IoT technology. In the rural conditions where the noise factor is approximately 5.0, the coverage is around 15 km, thus making it appropriate for the considered application.

When a sensor utilizes multi-tone transmission, the MCL is reduced to 158.23 dB. The only limiting factor for having better coverage is the battery consumption, which has to remain adequate. It is possible to use Class 5 (20 dBm) or Class 6 (14 dBm) devices that offer improved sensor lifespan.

Finally, addressing the feasibility of the considered commu-

TABLE III
INPUT PARAMETERS FOR NB-IOT LINK BUDGET CALCULATIONS.

Parameter	Uplink	Downlink
Transmit power, P_T	23 dBm	43 dBm
TX antenna gain, G_T	0 dBi	0 dBi
TX loss, L_T	0 dB	0 dB
Required SNR, $S_{\min}$	-6 dBm	-6 dBm
Channel bandwidth, B	3.75kHz 15kHz	180 kHz
Noise factor, N_F	3 dB	6 dB
RX antenna gain, G_R	0 dBi	0 dBi
RX losses, L_R	0 dBi	0 dBi

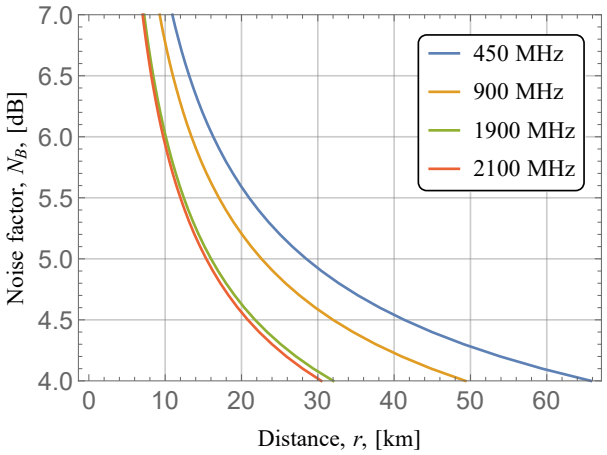

Fig. 7. Uplink coverage of NB-IoT.

nication schemes, one needs to take into account the effect of Earth curvature. The cargo vessels often sail in $10-20$ km proximity to the shore, see Fig. 1. Here, we also assume that the BS is located at 5 km distance from the coastline. In the most demanding DA scheme, NB-IoT devices on-board the ship will transmit the data directly. Recall that with the noise factor of 5.0 (corresponding to rural propagation conditions), the NB-IoT device and the BS coverage are 22 km and 30 km, respectively. Accounting for Earth curvature, as in Fig. 8, the LoS distance from the onshore BS, whose antenna is mounted at 30 m height, is approximately 20 km. Due to Earth curvature, the radio horizon distance from the transmitter to the receiver will actually be longer than the LoS. When the NB-IoT equipment is mounted on a cargo vessel, whose deck is approximately 20 m above the sea level, the combined radio horizon could be up to 41 km.

V. Performance Evaluation Framework

In this section, we develop a hybrid analytical-simulation framework for a performance assessment of the identified connectivity strategies. We first employ stochastic geometry to derive the connectivity properties with the coastal infrastructure and then proceed with formulating a simulation model that accounts for the NB-IoT access.

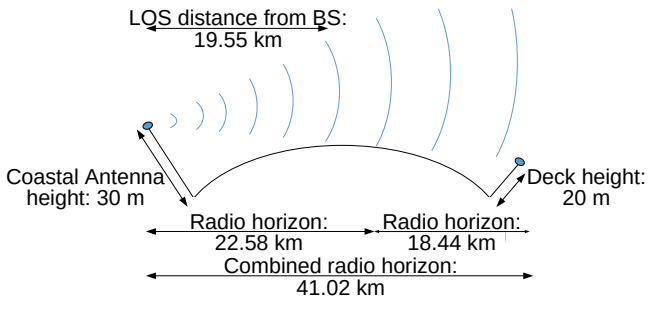

Fig. 8. Line-of-sight and radio horizons for DA scheme.

A. Connectivity Characterization

The communication with the onshore NB-IoT infrastructure is illustrated in Fig. 9 and Fig. 10. Note that the connectivity process with the coastal deployment can be classified as an alternating renewal process [80]. We need to determine the distributions of time for connectivity and outage periods to fully characterize this process. The main difficulty is related to the fact that the connectivity periods associated with individual BSs may overlap with each other, thus forming longer connectivity periods.

Let Λ be the intensity of BS projections on the vessel trajectory. Recall that the projection of a spatial PPP onto a random line forms a one-dimensional Poisson process [81]; then, the average intensity of the projected BSs is given by

$$\Lambda = \frac{\lambda_B}{B-A}\int_A^B f(x)dx, \tag{3}$$

where AB is the line segment on the ship trajectory, λ_B is the spatial density of onshore BSs, $f(x)$ is the function describing a coastal line. When the latter is nearly straight, we have $\Lambda = a\lambda_B$, where a is the width of the coast that can be reached from the ship, see Fig. 9.

Consider the distribution of the connectivity intervals created by a single BS, D. Using the notation in Fig. 9, we observe that $\cos\alpha = [(b+L)/r]$ leads to $\alpha = \cos^{-1}[(b+L)/r]$, where L is a random variable (RV) having the uniform distribution in $(0, a)$, r is the maximum NB-IoT BS coverage, and b is the distance between the ship and the coastal line. Furthermore, we see that $D/2 = (b+L)\tan\alpha$. Hence, we have the following for D

$$D = 2(b+L)\tan\cos^{-1}\left(\frac{b+L}{r}\right). \tag{4}$$

Observe that (4) is a non-linear transform of RV L. One may determine the probability density function (pdf) of D using the RV transformation technique [82]. Particularly, recall that the pdf of RV Y, $w(y)$, expressed as a function $y = \phi(x)$ of another RV X with the pdf $f(x)$ is given by

$$w(y) = \sum_{\forall i} f(\psi_i(y))|\psi_i'(y)|, \tag{5}$$

where $x = \psi_i(y) = \phi^{-1}(x)$, $i = 1, 2, \ldots$, are branches of the inverse function. The mean is then offered by

$$E[D] = \int_0^a 2(b+x)\tan\cos^{-1}\left(\frac{b+x}{r}\right)\frac{1}{a}dx, \tag{6}$$

which can be evaluated for any input parameters.

To characterize the outage and connectivity periods, we offer the following interpretation of the system at hand. Consider the connectivity periods created by the individual BSs as customers that arrive into a queuing system. Since the process of projections of the BS positions onto the trajectory of a ship is Poisson, this queuing system is associated with a Poisson arrival flow of customers with the intensity of Λ. Each customer requires the specific service time with the distribution of $f_D(x)$ as derived earlier, which implies that the system is associated with the generally distributed service times. Finally, since there may be infinitely many overlapping

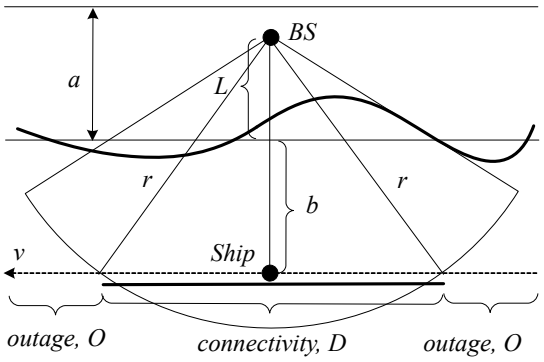

Fig. 9. Connectivity and outage for DA and SR schemes.

connectivity intervals, the system has to have infinite capacity. This queue is classified as M/GI/∞ in Kendall's nomenclature. Observe that the busy period in this system can be interpreted as the connectivity interval in our original system, while the uninterrupted period when there are no customers in the system constitutes the outage time.

The cumulative distribution function (CDF) of the busy period in the $M/GI/\infty$ queuing system is given by (7), which can be calculated numerically for any pdf of the connectivity periods with a single BS, $f_D(x)$ [83]. Furthermore, it directly follows from the renewal theory that the interval between two busy periods has an exponential distribution with the parameter Λ [80]. However, the calculations according to (7) constitute a complex process. To simplify the derivations, we approximate the M/GI/∞ queue as M/M/∞. For the latter, the busy period is distributed exponentially with the parameter

$$\theta = \frac{\Lambda}{(e^{-\Lambda/\mu} - 1)}, \tag{8}$$

where μ is the service intensity given by $\mu = 1/E[D]$.

Further, the geometry of the UAV relaying scheme is illustrated in Fig. 10. The key difference between the first two connectivity schemes and this one is that the coverage has to be evaluated for the UAV. To determine the connectivity period created by a single BS, one needs to distinguish the BSs located to the left or to the right of the UAV trajectory. Observing Fig. 10, we have

$$D_1 = 2\sqrt{r^2 - L_1^2},\ D_2 = 2\sqrt{r^2 - L_2^2}, \tag{9}$$

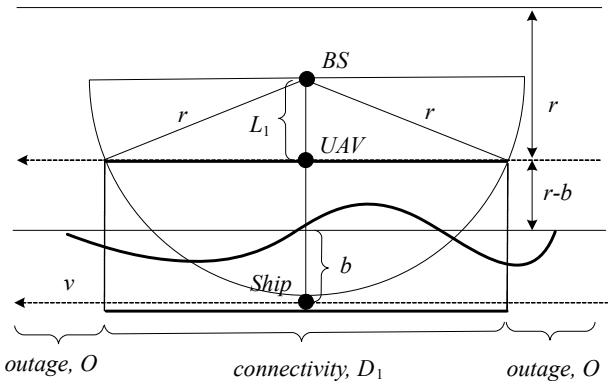

Fig. 10. Connectivity and outage for UR scheme.

where L_1 and L_2 are the distances between the UAV trajectory and the BSs located to the left or to the right of the UAV trajectory, respectively.

Employing the properties of the PPP deployment of BSs, one may observe that the probabilities that the BS is located to the right or to the left of the UAV trajectory are given by $r/(2r-b)$ and $(r-b)/(2r-b)$, respectively. Hence, the distribution of the connectivity periods is given by a weighed sum

$$f_D(x) = \frac{r}{2r-b} f_{D_1}(x) + \frac{r-b}{2r-b} f_{D_2}(x), \tag{10}$$

where $f_{D_1}(x)$ and $f_{D_2}(x)$ can be established by using (9) and applying the RV transformation technique according to (5).

However, since the mean value is readily given by

$$E[D] = \frac{r}{2r-b} \int_0^r \frac{2\sqrt{r^2-x^2}}{r} dx + \\ + \frac{r-b}{2r-b} \int_0^{r-b} \frac{2\sqrt{r^2-x^2}}{r-b} dx, \tag{11}$$

one may rely upon (8) by utilizing M/M/∞ approximation.

B. Random Access Analysis

To intuitively understand the behavior of our system, consider the typical time evolution of the mean message backlog for the DA scheme as the vessel moves along the coast, as shown in Fig. 11. Recall that the sensors compete for the BS transmission resources during the connectivity intervals, while no transmission attempts are performed during the outage periods. Therefore, the backlog increases as sensors generate messages following a Poisson process with the rate of λ during the outage intervals. When T_O is greater than T_S the messages are first accumulated by the system achieving a certain level as illustrated in Fig. 11 and then start to be dropped. Since messages are still generated by the sensors, the mean backlog plateaus. Once a connectivity period starts, sensors initiate their competition for the transmission resources, and the backlog decreases as a result of successful transmission attempts as well as drops caused by reaching the maximum number of retransmissions, M. The system eventually enters a stationary regime determined by the arrival rate, the amount of radio resources, and the NB-IoT random access procedure.

For the UAV and vessel relaying schemes, a local BS is always available, but the messages are further queued at the ship or at the UAV BSs and transmitted back-to-back when the onshore infrastructure becomes available. In all three cases, it is necessary to characterize the backlog at all of the time instants to describe the system dynamics, and further derive the loss and delay parameters. However, as one may observe in Fig. 11, the backlog dynamics is inherently non-stationary, thus making the system analytically intractable. As a result, one has to resort to computer simulations to derive the performance metrics of interest.

The developed modeling framework is based on discrete-event simulation (DES) techniques. The software is implemented by taking advantage of the Java programming language with multi-thread optimization [84]. The actual procedure

$$F_C(x) = 1 - \left[[1 - F_D(x)] \left[1 - \int_0^x (1 - F_C(x-z)) \exp(-\Lambda F_D(z)) \Lambda dz \right] + \int_0^x (1 - F_C(x-z)) \left| de^{-\Lambda F_D(z)} \right| \right]. \quad (7)$$

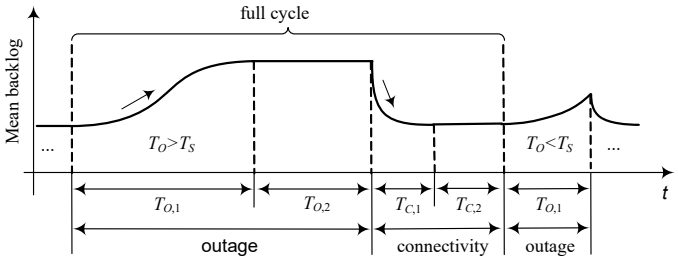

Fig. 11. Mean backlog dynamics for DA scheme.

comprises two phases: DES simulations and data analysis. Our developed DES framework implements the random access procedure with intermittent connectivity as described in this section followed by the data transmission.

A simulation campaign is then carried out to obtain the metrics of interest by relying upon the following procedure. Simulations are set to run for 10^6 seconds of the system time for every considered set of the input parameters. To remove any residual correlations in the statistical data, the batch means strategy is used. Accordingly, the entire steady-state period duration is divided into 1000 data blocks. The metrics of interest computed for these blocks are considered to be independent statistical samples. The final values of the parameters are estimated by processing these samples. Due to a large volume of statistical samples associated with our experiments, only the point estimates are shown in what follows. The reason is that the statistical interval estimates computed for the selected input parameters do not deviate by more than ± 0.01 from the absolute values of the respective point estimates under the level of significance set to $\alpha = 0.05$.

VI. Numerical Assessment

In this section, we assess the performance of our introduced scenarios. As the considered service is not of the real-time nature and, in fact, heavily depends on the network availability over the coastal area, the most critical parameter of interest is the message loss probability. Below, we start by addressing the message loss probability; then, we proceed to investigate the mean message delay; finally, we study the mean sensor lifetime. The input system parameters are provided in Table IV. We also note that by presenting the sensor lifetime estimates, we account for NB-IoT power consumption only. Hence, to achieve accurate results, the demonstrated numbers have to be appropriately scaled down by accounting for power consumption of the other end-system equipment. Furthermore, in our assessment, we have used the coin cell battery as an example. In real applications, the choice of the battery depends on many factors including the required current to power the wireless interface and other end-system elements.

Recall that for all of the considered connectivity schemes, a message loss may occur as a result of (i) reaching the maximum number of preamble retransmission attempts or (ii) reaching the maximum message lifetime. Hence, we begin by investigating how these individual components add up to form the overall message loss probability, as illustrated in Fig. 12 for the maximum number of preamble retransmissions set to $M = 10$ and the onshore NB-IoT BS density of $\lambda_B = 0.1$ units/km^2. Analyzing the collected data, one may observe that there is a fundamental difference between the loss components corresponding to the direct DA and the relay-based SR/UR connectivity schemes.

Notably, for all of the considered connectivity schemes, the losses induced by the excessive delay are significant, starting from around $\lambda = 0.1$ messages/h/sensor. The underlying reasons are in irregularities of the vessel coverage for a given choice of the message generation rate and the density of the onshore BSs. However, it is essential to emphasize that although for the DA and SR scenarios, the behaviors of the message loss probability curves are quite close, the UAV-based connectivity scheme is characterized by much milder losses. As for the possible explanation, the UAV is positioned closer to the onshore infrastructure, thus improving the vessel coverage by increasing the temporal intensity of the BSs.

According to the second component of the message loss process shown in Fig. 12, drops caused by exceeding the maximum number of preamble retransmissions are only experienced in the case of the DA scheme. For both SR and UR connectivity options, these losses are negligible. This behavior is explained by two positive effects of the SR/UR schemes: (i) temporal spreading of message transmission attempts at the sensor-to-vessel BS/UAV BS NB-IoT interfaces and (ii) multiplexing at the UAV/vessel BS-to-onshore BS NB-

TABLE IV
Default system parameters.

Parameter	Value
Operating frequency, f_C	900 MHz
Number of sensors, N	2000
Message arrival intensity, λ	1 message/h/sensor
Excess delay threshold, T_D	60 min
Number of RACH channels, C	48 channels
RACH periodicity, T_{RACH}	2560 ms
Number of RACH repetitions, K	128
Number of preamble retries, M	10
Battery capacity, E	1388 mAh (3.6 V)
Message frequency/day, F	8
Payload size, S	50 bytes
Coast width reachable from ship, a	8 km
Distance from ship to coastal line, b	10 km
NB-IoT BS coverage, r	18 km
Ship velocity, v	37 km/h

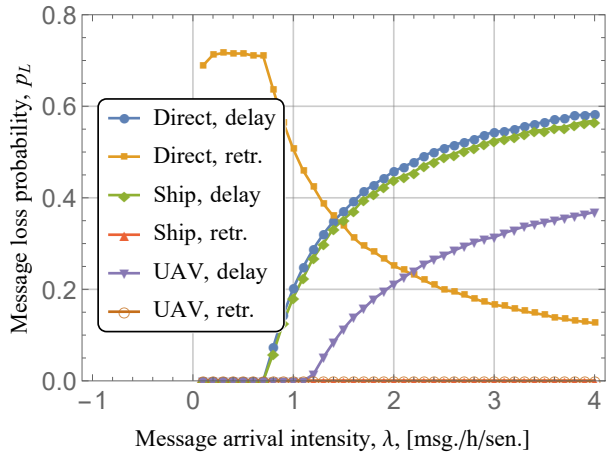

Fig. 12. Components of message loss process.

IoT interfaces.

Indeed, recalling that the connectivity periods are interchanging with long outage periods for all the three schemes, we observe that the sensors become synchronized in the DA case. Hence, once the vessel enters the coverage area of a new onshore BS, all of the sensors initiate their attempts to access the shared NB-IoT channel. Conversely, with the SR/UR schemes, the sensors remain de-synchronized while accessing the NB-IoT channel; this drastically reduces the probability of exceeding the maximum number of retransmissions. Furthermore, once the messages are transferred to the UAV BS/vessel BS, they join the shared queue and then travel sequentially, thus experiencing no competition for radio resources.

Consequently, we observe a decrease in message losses caused by exceeding the maximum number of preamble retransmissions for the DA scheme as drops caused by excessive delay grow. For smaller values of the message arrival intensity, we see that losses caused by the maximum number of retransmissions dominate. However, as the intensity increases and becomes higher than 1.5 message/h/sensor, the operating regime changes, and more drops are experienced as a result of the excessive delay. As an intermediate conclusion, we note that the SR/UR connectivity schemes efficiently alleviate the problem of synchronization at the air interfaces; this calls for no further collision avoidance mechanisms and highlights delay as the main factor affecting the message loss probability. Both factors play a significant role for the DA scheme.

We continue with investigating the behavior of the aggregate message loss process, which is illustrated in Fig. 13 as a function of the system parameters. Analyzing the impact of the message generation intensity, λ, we observe that for the DA scheme, it remains constant at approximately 0.7 for $M = 10$ and $\lambda_B = 0.1$. Note that extremely high message loss probabilities in light load conditions are explained by the fact that the sensors access the medium in a synchronized way. As the arrival intensity grows, the mean duration between the message generations as well as the message lifetime decrease, which leads the system to excessive delay dominated regime. For the SR/UR connectivity schemes, the message loss probability is negligibly low for smaller values of message generation intensity, but then it quickly increases as λ becomes higher. In fact, the behavior of the message loss process resembles that for the component induced by the excessive delay shown in Fig. 12.

The effect of the BS density on the message loss probability for $M = 10$, $\lambda = 1$ is demonstrated in Fig. 13(b). Recall that the growing spatial density of the BSs increases the duration of the connectivity intervals as well as reduces the outage times. As a result, we observe that the message loss probability decreases: this trend is strictly linear for all of the considered connectivity strategies. With the DA scheme, the message loss probability is unacceptable for practical systems even at extremely high BS densities on the order of 0.5 units/km^2. At the same time, the use of either relaying scheme allows for achieving efficient service from the message loss probability perspective across the realistic ranges of the BS intensities, i.e., smaller than 0.2 units/km^2. The use of the UR scheme further improves the system performance as it permits to increase the duration of the connectivity periods by enabling additional candidate BSs for more diverse connectivity.

The influence of the preamble retransmission attempts is illustrated in Fig. 13(c). Observe that a marginal performance improvement is observed when switching from $M = 1$ to $M = 2$ for all of the schemes. A further increase in M does not produce any substantial effect either. The main reason is in that the message losses are mainly affected by the connectivity process with the onshore BSs for all the considered schemes.

Further, we proceed with assessing the delay performance of our system. Fig. 14 shows the effects of the system parameters on the mean delay between the sensor and the onshore BS. Analyzing the data illustrated in Fig. 14(a), we learn that the best performance is observed for the DA connectivity scheme. This behavior is explained by the fact that most of the messages arriving during the outage period are eventually lost as a result of two factors: relatively long outage periods and high contention at the beginning of a connectivity period. Since the delay in question is the mean delay conditioned on a successful message delivery, the resultant values for the DA scheme in Fig. 14(a) reflect only the situations, where a message arrives in the middle or towards the end of a connectivity interval, and thus experiences no severe contention. In these circumstances, the system is underloaded, and arriving messages are, in most cases, delivered successfully to the onshore BS. The described behavior is a dominating factor for all of the illustrated dependencies related to the DA scheme in Fig. 14.

Continuing with the SR/UR schemes, one may observe a peculiar behavior of the mean delay as a function of the message arrival intensity in Fig. 14(a). Notably, for both alternatives, the mean delay first increases and then – starting from a particular value of λ – begins to decrease. The underlying reason for this behavior is that the system experiences relatively low loss probability as a result of excessive delay tolerating outage intervals up to a turning point. Growing arrival intensity in these intervals will lead to the conventional behavior of a stable system – the mean delays increases. However, when a specific limit of the message arrival intensity is reached, losses begin to accumulate, see Fig. 13(a), and the mean delay

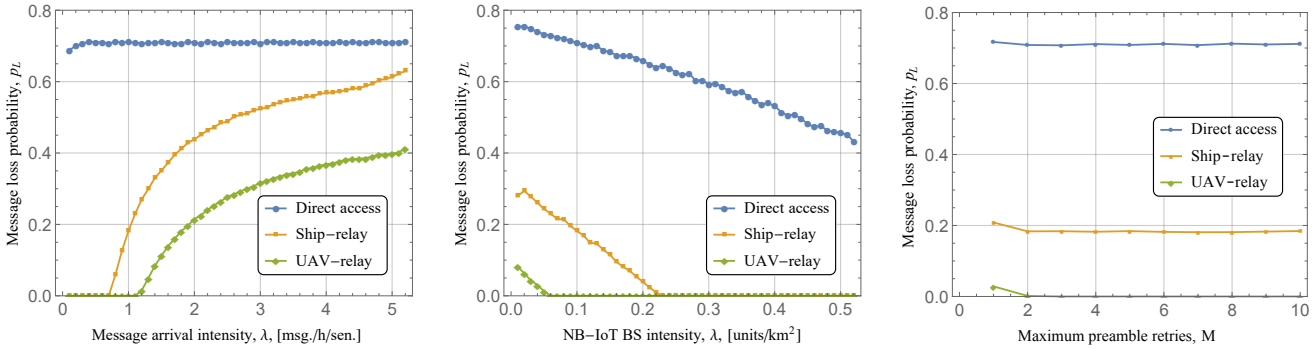

(a) As function of offered traffic load (b) As function of BS intensity (c) As function of preamble attempts

Fig. 13. Message loss probability as function of system parameters.

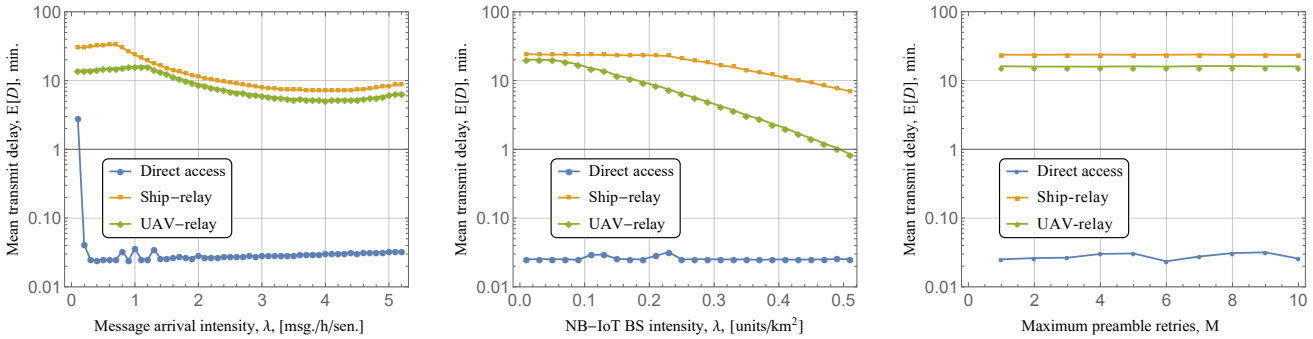

(a) As function of offered traffic load (b) As function of BS intensity (c) As function of preamble attempts

Fig. 14. Mean delay as function of system parameters.

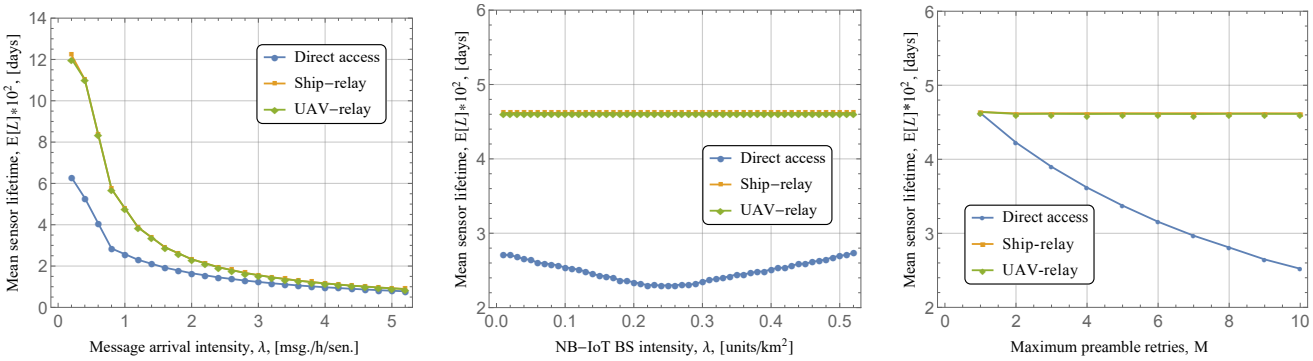

(a) As function of offered traffic load (b) As function of BS intensity (c) As function of preamble attempts

Fig. 15. Mean sensor lifetime as function of system parameters.

decreases drastically.

The effects of the onshore BS density on the mean delay are highlighted in Fig. 14(a). Understanding the presented data, one may learn that the mean delay exhibits intricate behavior for the SR/UR schemes. It remains nearly constant for a certain density of the BSs and then starts to decrease. This is mainly because most of the outage intervals are long enough to induce losses as a result of excessive message delay up to this turning point. Once the BS density is such that the mean outage intervals become shorter than $1/\lambda$, not only message loss probability but also mean delay decrease. Finally, similar to message loss probability, no noticeable effect of the number of preamble retransmissions on the mean delay is observed, as one may deduce from Fig. 14(c).

Finally, we analyze the impact of the system parameters on the sensor lifetime, see Fig. 15. Recall that to produce these values, we assumed having a typical 'coin' cell battery with a capacity of 1388 mAh (3.6 V), which is often used in sensor equipment [85]. First, we note that the sensor lifetimes for the SR and UR schemes are almost identical as they both utilize the relaying approach. Second, the SR/UR schemes are preferred in terms of the sensor lifetime as compared to the DA option. The reason is that for the former schemes, the transmissions at the sensor-to-relay interface are de-synchronized, which implies that fewer preamble retransmission attempts are required for a message delivery. Analyzing the dependence on the message arrival rate illustrated in Fig. 15(a), one may conclude that the sensor lifetime decreases for all the three

considered connectivity alternatives. However, even for higher arrival intensities, e.g., $2-3$ messages per hour per sensor, the mean sensor lifetime remains approximately 200 days. When at most 1 message is generated per hour, the relay-based SR and UR schemes may lead to over a year-long operation.

It is essential to note that the density of the onshore BSs and the maximum number of retransmissions do not produce any noticeable effect on the sensor lifetime for the SR/UR connectivity schemes. The explanation is in that due to relatively long outage intervals for the considered connectivity schemes (and for practical system parameters), the sensors spend most of their time in the "ready-to-transmit" state. Notably, an increase in the lifetimes is only observed for impractical BS densities. This is also the reason why the lifetime is insensitive to the number of retransmission attempts, despite that, the energy spent for the actual transmissions is much higher compared to that required in the ready-to-transmit state, the fraction of time that a sensor actually transmits is insignificant.

The behavior of sensor lifetime for the DA scheme is more complex, see Fig. 15(b) and Fig. 15(c). Notably, as the BS density increases, the lifetime first drops and then reaches a turning point where a further increase in λ_B leads to longer lifetimes. The reason here is that an increase in λ_B decreases the duration of outage intervals, and more sensors have an opportunity for a data transmission. However, these transmissions are in most cases unsuccessful, thus consuming the maximum possible amount of power during a sensor duty cycle due to the synchronization effect. However, when the BS density becomes more distinguished than a threshold value, longer connectivity intervals begin to affect the sensor lifetimes positively. Particularly, the message loss probability and the mean delay decrease as observed in Fig. 13(c) and Fig. 14(c), which implies that less energy is spent on average for a single message transmission. Finally, the explanation behind decreased sensor lifetimes in response to growing maximum number of preamble retransmissions is such that with this scheme most of the messages are delivered unsuccessfully – irrespective of the number of attempts – thus requiring the maximum amount of energy to be spent during a sensor duty cycle.

VII. Conclusions

In this paper, we envisioned the exploitation of the onshore NB-IoT infrastructure for tracking numerous containers carried by marine cargo vessels. We considered three candidate connectivity schemes, including a direct sensor to the onshore BS communication capability and two relaying strategies that utilize the vessel's onboard BS and the UAV-mounted BS, respectively. To assess and compare the performance of the introduced strategies, we analyzed the message loss probability, the mean message delay, and the sensor lifetime as our key performance metrics. Finally, we developed an efficient analytical-simulation framework for the purposes of this evaluation campaign.

Our numerical results indicated that the direct access scheme is characterized by the worst performance out of all the considered options. The underlying reason is that the interchanging connectivity and outage periods with the onshore NB-IoT infrastructure lead to enforced synchronization effects that severely deteriorate the performance indicators. The relay-based strategies allow to significantly improve the system performance by effectively distributing the device transmission requests over time at the sensor-to-relay air interface, while further benefiting from no contention at the onshore BS air interface. Additional gains delivered by employing the UAV relays are related to extending the onshore coverage, thus increasing the levels of BS density.

The resultant system performance heavily depends on the density of the onshore BS deployment. However, the considered relaying mechanisms, especially the one based on the UAV-aided transmissions, may help mitigate the harmful connectivity interruptions across a wide range of input parameters. Utilizing the globally standardized NB-IoT communications and complementing it with the rapidly maturing drone technology, we believe that the proposed operation can be employed in conjunction with the conventional tracking techniques, such as those using satellite communications, to decrease the operational expenditures of marine cargo vessels.

VIII. Acknowledgments

This work was supported by the Academy of Finland (projects PRISMA and RADIANT) as well as by the projects aColor, 5G-FORCE, and RAAS Connectivity RTF framework.

References

[1] International Maritime Organization (IMO), "Marine Environment," *[Online]*, 2019.
[2] GT Staff, "Smart Shipping Container Technology Comes to North America," *Global Trade Magazine*, Dec 2017.
[3] Budget Shipping Containers, "How many Shipping Containers are there in the World?" *[Online]*, Mar 2016.
[4] ISL; Marine Flottenkommando, "Number of ships in the world merchant fleet between January 1, 2008 and January 1, 2017, by type," *[Online]*, 2018.
[5] Statista, "Container Shipping – Statistics & Facts," *[Online]*, 2019.
[6] World Shipping Council., "Containers Lost At Sea – 2017 Update," *[Online]*, 2017.
[7] TMC Marine – a burey veritas group company, "Top 25 causes of container claims," *[Online]*, 2017.
[8] E. Maras, "IoT Technology Uplifts Container Tracking," *Food Logistics*, Oct 2016.
[9] S. Mahlknecht and S. A. Madani, "On architecture of low power wireless sensor networks for container tracking and monitoring applications," in *Proc. of 5th IEEE International Conference on Industrial Informatics*, vol. 1. IEEE, 2007, pp. 353–358.
[10] P. P. Ray, "A survey on Internet of Things architectures," *Journal of King Saud University-Computer and Information Sciences*, vol. 30, no. 3, pp. 291–319, 2018.
[11] Z. D. R. Gnimpieba, A. Nait-Sidi-Moh, D. Durand, and J. Fortin, "Using Internet of Things technologies for a collaborative supply chain: Application to tracking of pallets and containers," *Procedia Computer Science*, vol. 56, pp. 550–557, 2015.
[12] E. D. N. Ndih and S. Cherkaoui, "On enhancing technology coexistence in the IoT Era: ZigBee and 802.11 case," *IEEE Access*, vol. 4, pp. 1835–1844, 2016.
[13] R. Harwahyu, R.-G. Cheng, W.-J. Tsai, J.-K. Hwang, and G. Bianchi, "Repetitions vs Retransmissions: Trade-off in Configuring NB-IoT Random Access Channels," *IEEE Internet of Things Journal*, 2019.
[14] R. S. Sinha, Y. Wei, and S.-H. Hwang, "A survey on LPWA technology: LoRa and NB-IoT," *ICT Express*, vol. 3, no. 1, pp. 14–21, 2017.
[15] 3GPP TS 36.101, "LTE; Evolved Universal Terrestrial radio access (E-UTRA); User equipment (UE) radio transmission and reception," ETSI, Report P-32, 2016.

[16] V. Tikhvinskiy, G. Bochechka, A. Gryazev, and A. Aitmagambetov, "Comparative Analysis of QoS Management and Technical Requirements in 3GPP Standards for Cellular IoT Technologies," *Journal of Telecommunications and Information Technology*, no. 2, pp. 41–47, 2018.

[17] V. Petrov, A. Samuylov, V. Begishev, D. Moltchanov, S. Andreev, K. Samouylov, and Y. Koucheryavy, "Vehicle-based relay assistance for opportunistic crowdsensing over narrowband IoT (NB-IoT)," *IEEE Internet of Things Journal*, vol. 5, no. 5, pp. 3710–3723, 2017.

[18] T. Xu and I. Darwazeh, "Non-orthogonal narrowband Internet of Things: A design for saving bandwidth and doubling the number of connected devices," *IEEE Internet of Things Journal*, vol. 5, no. 3, pp. 2120–2129, 2018.

[19] B. Li, Y. Jiang, J. Sun, L. Cai, and C.-Y. Wen, "Development and testing of a two-UAV communication relay system," *Sensors*, vol. 16, no. 10, p. 1696, 2016.

[20] J. Pokorny, A. Ometov, P. Pascual, C. Baquero, P. Masek, A. Pyattaev, A. Garcia, C. Castillo, S. Andreev, J. Hosek *et al.*, "Concept design and performance evaluation of UAV-based backhaul link with antenna steering," *Journal of Communications and Networks*, vol. 20, no. 5, pp. 473–483, 2018.

[21] T. Michael, "New Maersk smart containers can listen and talk," *Dynamic Export [Online]*, 2016.

[22] Vobal Technologies, "GSM Service For The Commercial Shipping Industry," *[Online]*, 2019.

[23] ORBCOMM, "RCU – Remote Container Management," *Technical Specification [Online]*, 2016.

[24] ZIM Integrated Shipping Services Ltd., "ZIMonitor," *Technical Specification [Online]*, 2019.

[25] E. Tanghe, W. Joseph, P. Ruckebusch, L. Martens, and I. Moerman, "Intra-, inter-, and extra-container path loss for shipping container monitoring systems," *IEEE Antennas and Wireless Propagation Letters*, vol. 11, pp. 889–892, 2012.

[26] R. J. Katulski, J. Sadowski, J. Stefański, and S. J. Ambroziak, "Self-organizing wireless monitoring system for cargo containers," *Polish Maritime Research*, pp. 45–50, 2009.

[27] T. Bretschneider and N. Thai Dung, "Container tracking via AIS satellites," in *Proc. of Asian Conference on Remote Sensing, Myanmar*, 2014.

[28] B. Ray, "Container Tracking Systems: Everything You Need To Know," *LinkLabs Company Blog [Online]*, 2018.

[29] A. Klimkowska, I. Lee, and K. Choi, "Possibilities of UAS for maritime monitoring," *The International Archives of Photogrammetry, Remote Sensing and Spatial Information Sciences*, vol. 41, p. 885, 2016.

[30] European Maritime Safety Agency, "EMSA RPAS drone service to boost maritime surveillance in Croatia," *[Online]*, July 2019.

[31] Royal Institution of Naval Architects, "UAV (drone) inspection: Shiprepair & Maintenance: eNews February 2017," *[Online]*, 2017.

[32] HighEye, "Detailed inspection of ocean-based assets from shore-based locations," *[Online]*, 2018.

[33] The Shephard News Team, "Martek expands into maritime UAS market," *[Online]*, November 2017.

[34] Wilhelmsen Ships Service, "Wilhelmsen unveils agency by air at NorShipping," *[Online]*, May 2017.

[35] S. O'Young and P. Hubbard, "RAVEN: A maritime surveillance project using small UAV," in *Proc. of IEEE Conference on Emerging Technologies and Factory Automation (EFTA 2007)*. IEEE, 2007, pp. 904–907.

[36] H. Alzu'bi, I. Mansour, and O. Rawashdeh, "Loon Copter: Implementation of a hybrid unmanned aquatic–aerial quadcopter with active buoyancy control," *Journal of Field Robotics*, vol. 35, no. 5, pp. 764–778, 2018.

[37] C. Castillo, A. Pyattaev, J. Villa, P. Masek, D. Moltchanov, and A. Ometov, "Autonomous UAV Landing on a Moving Vessel: Localization Challenges and Implementation Framework," in *Internet of Things, Smart Spaces, and Next Generation Networks and Systems*. Springer, 2019, pp. 342–354.

[38] Verdict Media Limited, "Skeldar V-200 Maritime Unmanned Aerial Vehicle (UAV)," [Online], 2019.

[39] i-HLS, "Triton UAV to Enhance US Maritime Surveillance," [Online], November 2017.

[40] P. McLearly, "Navy's New Triton Drone Heads To Guam, New Pacific Recon Tool," Breaking Media, Inc., September 2019.

[41] J. M. Kelner, C. Ziółkowski, and L. Nowosielski, "Local navigation system for VTOLs used on the vessels," in *Proc. of IEEE/ION Position, Location and Navigation Symposium (PLANS)*. IEEE, 2016, pp. 415–421.

[42] H. Y. Irwanto, "HILS of auto take off system: For high Speed UAV using booster rocket," in *Proc. of International Seminar on Intelligent Technology and Its Applications (ISITIA)*. IEEE, 2016, pp. 373–380.

[43] Z. Novaković, N. Medar, and L. Mitrović, "Increasing launch capability of a UAV bungee catapult," *Scientific technical review*, vol. 64, no. 4, pp. 17–26, 2014.

[44] L. Yue and Z. Haili, "Principle experiments of hydraulic and pneumatic launching of UAV," *Journal of Nanjing University of Aeronautics & Astronautics*, vol. 6, 2010.

[45] W. R. McDonnell and C. H. Baker, "Launch and recovery system for unmanned aerial vehicles," Aug. 27 2013, US Patent 8,517,306.

[46] M. Laiacker, S. Wlach, and M. Schwarzbach, "DLR High altitude balloon launched experimental glider (HABLEG): system design, control and flight data analysis," in *Proc. of Workshop on Research, Education and Development of Unmanned Aerial Systems (RED-UAS)*. IEEE, 2015, pp. 360–368.

[47] M. A. Watts, G. R. Root Jr, and D. M. Adamski, "UAV recovery system," May 22 2007, US Patent 7,219,856.

[48] R. W. Barthelme, J. B. Leonard, and J. N. Biercuk, "Ship compatible launch, retrieval and handling system for (VTOL) aircraft," Dec. 2 1980, US Patent 4,236,686.

[49] J. Snediker, M. A. Watts, and G. W. Corboy, "UAV arresting hook for use with UAV recovery system," Dec. 5 2006, US Patent 7,143,976.

[50] G. H. Lovell, E. C.-K. Hui, and M. K. Umbreit, "Stabilized UAV recovery system," May 8 2012, US Patent 8,172,177.

[51] L. G. Carrillo, E. Rondon, A. Sanchez, A. Dzul, and R. Lozano, "Stabilization and trajectory tracking of a quad-rotor using vision," *Journal of Intelligent & Robotic Systems*, vol. 61, no. 1-4, pp. 103–118, 2011.

[52] A. Gautam, P. Sujit, and S. Saripalli, "A survey of autonomous landing techniques for UAVs," in *Proc. of International conference on unmanned aircraft systems (ICUAS)*. IEEE, 2014, pp. 1210–1218.

[53] B. Rao, A. G. Gopi, and R. Maione, "The societal impact of commercial drones," *Technology in Society*, vol. 45, pp. 83–90, 2016.

[54] S. Pappu, Y. Liu, J. F. Horn, and J. Cooper, "Wind gust estimation on a small VTOL UAV," in *Proc. of 7th AHS Technical Meeting on VTOL Unmanned Aircraft Systems*. American Helicopter Soc. Fairfax, VA, 2017, pp. 1–19.

[55] C. Zhang, X. Zhou, H. Zhao, A. Dai, and H. Zhou, "Three-dimensional fuzzy control of mini quadrotor UAV trajectory tracking under impact of wind disturbance," in *Proc. of International Conference on Advanced Mechatronic Systems (ICAMechS)*. IEEE, 2016, pp. 372–377.

[56] B. Rubí, R. Pérez, and B. Morcego, "A Survey of Path Following Control Strategies for UAVs Focused on Quadrotors," *Journal of Intelligent & Robotic Systems*, pp. 1–25, 2019.

[57] I. Siti, M. Mjahed, H. Ayad, and A. El Kari, "New Trajectory Tracking Approach for a Quadcopter Using Genetic Algorithm and Reference Model Methods," *Applied Sciences*, vol. 9, no. 9, p. 1780, 2019.

[58] M. Faria, J. Pinto, F. Py, J. Fortuna, H. Dias, R. Martins, F. Leira, T. A. Johansen, J. Sousa, and K. Rajan, "Coordinating UAVs and AUVs for oceanographic field experiments: Challenges and lessons learned," in *Proc. of IEEE International Conference on Robotics and Automation (ICRA)*. IEEE, 2014, pp. 6606–6611.

[59] R. Weibel and R. J. Hansman, "Safety considerations for operation of different classes of UAVs in the NAS," in *Proc. of 4th Aviation Technology, Integration and Operations (ATIO) Forum*, 2004, p. 6244.

[60] R. Hann, A. Wenz, K. Gryte, and T. A. Johansen, "Impact of atmospheric icing on UAV aerodynamic performance," in *Proc. of Workshop on Research, Education and Development of Unmanned Aerial Systems (RED-UAS)*. IEEE, 2017, pp. 66–71.

[61] M. M. Marques, P. Dias, N. P. Santos, V. Lobo, R. Batista, D. Salgueiro, A. Aguiar, M. Costa, J. E. da Silva, A. S. Ferreira *et al.*, "Unmanned Aircraft Systems in Maritime Operations: Challenges addressed in the scope of the SEAGULL project," in *Proc. of OCEANS 2015-Genova*. IEEE, 2015, pp. 1–6.

[62] Y.-P. E. Wang, X. Lin, A. Adhikary, A. Grovlen, Y. Sui, Y. Blankenship, J. Bergman, and H. S. Razaghi, "A primer on 3GPP narrowband Internet of Things," *IEEE Communications Magazine*, vol. 55, no. 3, pp. 117–123, 2017.

[63] A. Adhikary, X. Lin, and Y.-P. E. Wang, "Performance evaluation of NB-IoT coverage," in *Proc. of IEEE 84th Vehicular Technology Conference (VTC-Fall)*. IEEE, 2016, pp. 1–5.

[64] M. Lauridsen, I. Z. Kovács, P. Mogensen, M. Sorensen, and S. Holst, "Coverage and capacity analysis of LTE-M and NB-IoT in a rural area," in *Proc. of IEEE 84th Vehicular Technology Conference (VTC-Fall)*. IEEE, 2016, pp. 1–5.

[65] Y. Miao, W. Li, D. Tian, M. S. Hossain, and M. F. Alhamid, "Narrowband Internet of Things: simulation and modeling," *IEEE Internet of Things Journal*, vol. 5, no. 4, pp. 2304–2314, 2017.

[66] Y. D. Beyene, R. Jantti, K. Ruttik, and S. Iraji, "On the performance of narrow-band Internet of Things (NB-IoT)," in *Proc. of IEEE Wireless Communications and Networking Conference (WCNC)*. IEEE, 2017, pp. 1–6.

[67] M. Lauridsen, H. Nguyen, B. Vejlgaard, I. Z. Kovács, P. Mogensen, and M. Sorensen, "Coverage Comparison of GPRS, NB-IoT, LoRa, and SigFox in a 7800 km^2 Area," in *Proc. of IEEE 85th Vehicular Technology Conference (VTC Spring)*. IEEE, 2017, pp. 1–5.

[68] B. Vejlgaard, M. Lauridsen, H. Nguyen, I. Z. Kovács, P. Mogensen, and M. Sorensen, "Coverage and Capacity Analysis of Sigfox, LoRa, GPRS, and NB-IoT," in *Proc. of IEEE 85th vehicular technology conference (VTC Spring)*. IEEE, 2017, pp. 1–5.

[69] S. Cluzel, L. Franck, J. Radzik, S. Cazalens, M. Dervin, C. Baudoin, and D. Dragomirescu, "3GPP NB-IoT coverage extension using LEO satellites," in *Proc. of IEEE 87th Vehicular Technology Conference (VTC Spring)*. IEEE, 2018, pp. 1–5.

[70] M. El Soussi, P. Zand, F. Pasveer, and G. Dolmans, "Evaluating the performance of eMTC and NB-IoT for smart city applications," in *Proc. of IEEE International Conference on Communications (ICC)*. IEEE, 2018, pp. 1–7.

[71] N. Mangalvedhe, R. Ratasuk, and A. Ghosh, "NB-IoT deployment study for low power wide area cellular IoT," in *Proc. of IEEE 27th Annual International Symposium on Personal, Indoor, and Mobile Radio Communications (PIMRC)*. IEEE, 2016, pp. 1–6.

[72] R. Ratasuk, B. Vejlgaard, N. Mangalvedhe, and A. Ghosh, "NB-IoT system for M2M communication," in *Proc. of IEEE wireless communications and networking conference*. IEEE, 2016, pp. 1–5.

[73] K. William, "How much bigger can container ships get?" *BBC News Magazine*, 2013.

[74] J. F. C. Kingman, *Poisson processes*. Clarendon Press, 1992, vol. 3.

[75] S. Xu, Y. Liu, and W. Zhang, "Grouping-based discontinuous reception for massive narrowband Internet of Things systems," *IEEE Internet of Things Journal*, vol. 5, no. 3, pp. 1561–1571, 2018.

[76] N. Jiang, Y. Deng, M. Condoluci, W. Guo, A. Nallanathan, and M. Dohler, "RACH preamble repetition in NB-IoT network," *IEEE Communications Letters*, vol. 22, no. 6, pp. 1244–1247, 2018.

[77] ISO, "Freight containers – Container Tracking and Monitoring Systems (CTMS): Requirements," Report TS 18625:2017(E), October 2017.

[78] X. Lin, A. Adhikary, and Y.-P. E. Wang, "Random access preamble design and detection for 3GPP narrowband IoT systems," *IEEE Wireless Communications Letters*, vol. 5, no. 6, pp. 640–643, 2016.

[79] R. Ratasuk, N. Mangalvedhe, Y. Zhang, M. Robert, and J.-P. Koskinen, "Overview of narrowband IoT in LTE Rel-13," in *Proc. of IEEE Conference on Standards for Communications and Networking (CSCN)*. IEEE, 2016, pp. 1–7.

[80] D. R. Cox, *Renewal theory*. Methuen London, 1967, vol. 1.

[81] S. N. Chiu, D. Stoyan, W. S. Kendall, and J. Mecke, *Stochastic geometry and its applications*. John Wiley & Sons, 2013.

[82] S. M. Ross, *Introduction to probability models*. Academic press, 2014.

[83] D. J. Daley and L. Servi, "Idle and busy periods in stable M/M/k queues," *Journal of applied probability*, vol. 35, no. 4, pp. 950–962, 1998.

[84] B. P. Zeigler, T. G. Kim, and H. Praehofer, *Theory of modeling and simulation*. Academic press, 2000.

[85] iNELS Air, "Sensors and detectors for IoT," *Product Brochure [Online]*, 2019.